Title

Numerical Monte Carlo Simulations to Evaluate the Influence That Spherical Nanoparticle Size and Arrangement Have on Interparticle Charge Transport across the Surface of Dye- and Cocatalyst-Modified Materials

Journal

ACS Applied Energy Materials, 3(5)

ISSN

2574-0962

Authors

Tkaczibson, Kevin

Ardo, Shane

Publication Date

2020-05-26

DOI

10.1021/acsaem.0c00336

ACS APPLIED ENERGY MATERIALS

www.acsaem.org Article

Numerical Monte Carlo Simulations to Evaluate the Influence That Spherical Nanoparticle Size and Arrangement Have on Interparticle Charge Transport across the Surface of Dye- and Cocatalyst-Modified Materials

Kevin Tkaczibson and Shane Ardo*

Cite This: *ACS Appl. Energy Mater.* 2020, 3, 4699−4707 Read Online

ACCESS | Metrics & More | Article Recommendations | Supporting Information

ABSTRACT: Mechanistic information underlying the function of illuminated mesoporous thin films of nanomaterials that contain distinct light-absorbing and electrocatalytic units can be gleaned from discrete-time random walk Monte Carlo simulations. These simulations bridge the length and time scales between individual electron-transfer events and ensemble behavior observed from bulk thin films. Most simulations are performed using models that simplify random mesoporous networks as isolated spherical nanoparticles. However, these simplifications may not provide sufficient detail to capture macroscopic experimental observations, especially when mesoporous nanomaterials consist of various geometries. Herein, we examine the role that the structure of the mesoporous thin film plays on the ability of photogenerated charges to accumulate on surface-confined redox-active electrocatalysts that require two redox events for turnover. We observe that the structure has a dramatic influence on the expected spectroscopic absorption anisotropy signal over time. We also observe that the yield for electrocatalyst turnover, as a function of the ratio of the electron-transfer time constant for self-exchange reactions and charge recombination time constant between the semiconducting mesoporous thin film and an oxidized/reduced surface-confined dye or electrocatalyst, is influenced by the total surface coverage of redox-active species. Structures consisting of spherical nanoparticles that are barely touching or partially necked are more effective at electrocatalytic turnover in the presence of vacant sites than discrete spherical nanoparticles or those that are arranged in a rodlike structure. Moreover, we show that the yield for electrocatalyst turnover is nearly independent of whether the simulations are performed on complex three-dimensional structures or simple two-dimensional planar grids. This discovery suggests that the added complexity of three-dimensional models may not be necessary to explain differences in electrocatalytic turnover yield in photoelectrochemical constructs containing surface-confined light-absorbing and electrocatalytic units.

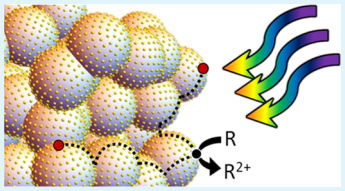

KEYWORDS: *dye sensitization, dye-sensitized photoelectrochemical cells, Monte Carlo simulations, self-exchange reactions, hole hopping, charge accumulation*

INTRODUCTION

Solar fuel constructs consisting of nanoparticles adorned with discrete light absorbers and discrete electrocatalysts must effectively transport charge to electrocatalysts to activate them for desired reactivity.[1,2] Optimally, the rate of electron-transfer recombination between the nanoparticle and an oxidized/reduced dye or electrocatalyst should be slow, the rate of electron transfer between surface-confined redox-active species should be fast, and the rate of electrocatalytic turnover should be fast. Electron-transfer recombination and surface-confined electron transport processes have been studied extensively for materials with discrete visible-light-absorbing moieties, and various standard structures have been simulated using Monte Carlo methods.[3−24] Only recently did we report analogous models that also included electrocatalytic units,[25] where we identified the conditions for optimal light-driven electrocatalytic turnover. The models used in that work, and in most other works that do not contain electrocatalysts, typically consist of particles modeled as discrete three-dimensional spheres, two-dimensional sheets, or one-dimensional lines, without the possibility for interparticle charge transport. However, many materials consist of structures that deviate from these simple geometries and afford pathways for interparticle charge transport, whether it be via through-space electronic wavefunction overlap, physical sintering of particles to generate nanoscale necking regions, or even alternative shapes formed from clusters of nanometer-sized particles. Therefore, inclusion of the possibility for interparticle charge transport in numerical Monte Carlo simulations may be important for replicating experimental observations made using mesoporous thin films.

Received: February 15, 2020
Accepted: March 18, 2020
Published: March 18, 2020

https://dx.doi.org/10.1021/acsaem.0c00336
ACS Appl. Energy Mater. 2020, 3, 4699−4707

Several groups have modeled thin films of dye-sensitized semiconducting nanoparticles as detailed three-dimensional mesoporous networks of spheres to simulate electron transport within the semiconducting materials and interfacial electron-transfer recombination processes.[26−37] However, in none of those works was surface-confined electron transfer between redox-active molecules anchored to the nanoparticle surfaces considered. Uniquely, only Meyer and co-workers simulated electron-transfer processes between molecules surface-anchored to a three-dimensional structure consisting of a regular array of spherical nanoparticles using a discrete-time random walk Monte Carlo method.[8] Inclusion of interparticle electron transfer between surface-anchored molecules led to simulated kinetic behavior that exhibited a long-time tail to the recombination kinetics, which more closely mimicked results observed from transient absorption spectroscopy measurements.

Herein, we expand on our previous model, which consisted of discrete spherical particles, to include structures where the particles touch and/or overlap, even to the extreme of being rodlike, thus allowing for interparticle electron transfer via the bulk semiconducting support and surface-confined redox-active species. These structures represent more realistic mesoporous networks whose impacts on pulsed-light-induced surface transport between discrete light absorbers and discrete electrocatalysts requiring two redox events for turnover are reported. We evaluate the effect that these structures have on electrocatalyst turnover as a function of self-exchange electron-transfer time constant, electron-transfer recombination time constant, excitation light intensity, optical polarization, and the percentage of molecular positions that are vacant on the particle surface. Results from this work will further guide the design of light-absorbing materials that efficiently utilize photons to drive chemical transformations at discrete electrocatalytic sites, which is of particular relevance to dye-sensitized solar cells that utilize the iodide/triiodide redox mediator. If this two-electron-transfer redox reaction could be driven rapidly at low overpotential, the efficiency of dye-sensitized solar cells that utilize the iodide/triiodide redox mediator could increase substantially.[3]

EXPERIMENTAL SECTION

Modeling Framework. The modeling framework aims to simulate the structure of thin films of nanomaterials with surface-bound electrocatalytic and light-absorbing units (Figure 1). Computer code to generate the models and perform the simulations, written in both Mathematica and Python, is available in ref 38. The underlying framework for this model and simulation process is generally the same as that used in our prior study where only discrete spherical particles were used,[25] but with several significant modifications as noted below and, for convenience, with the previous model briefly described here. Experimentally, thin films of mesoporous TiO_2 used in photoelectrochemical constructs are coated with dye molecules and electrocatalyst molecules. The modeling framework captures this behavior by creating a distribution of molecular surface sites and assigning each as a dye, catalyst, or nothing. Initially, some dye molecules on the simulated surface are randomly assigned as oxidized/reduced due to presumed photoexcitation and excited-state electron-transfer events. The simulation proceeds by effectively waiting for a time period that is >90 times shorter than the time constant for self-exchange electron transfer or charge recombination and then allowing each oxidized/reduced molecular charge on the surface to move to an adjacent molecule via presumed self-exchange electron transfer, to recombine with an electron/hole injected into the bulk of the semiconductor support, or to remain stationary. The probabilities for each of these events are predetermined during simulation initialization based on input time-constant values. In general, the outcome of interest is the yield for electrocatalyst turnover, which is defined based on the number of oxidized/reduced molecular charges created through photoexcitation events that ultimately results in complete oxidation/reduction of electrocatalysts.

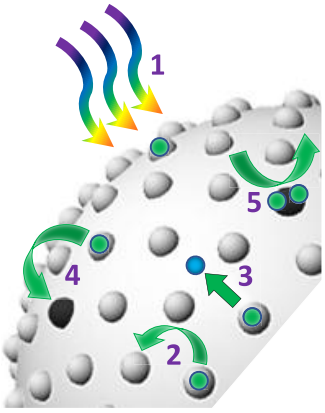

Figure 1. Depiction of the processes included in the modeling framework: (1) dye photoexcitation, (2) self-exchange electron transfer, (3) charge recombination, (4) electron transfer between dyes and electrocatalysts, and (5) electrocatalytic turnover.

Three-Dimensional Structures. The primary focus of our work herein was to model and simulate several structures and other related surface conditions. Evaluation of these new structures and surface conditions is important because they represent more physically relevant scenarios encountered experimentally when studying typical mesoporous thin films utilized in dye-sensitized photoelectrochemical constructs. The use of several structures differs from our prior study where only one structure was modeled, which consisted of a stack of spherical particles that were not in physical contact and thus the particles only influenced each other in some cases through competitive light absorption. The main three-dimensional structures modeled herein are shown in Figure 2. Most of these structures consist of truncated spheres that are in physical contact, thus allowing molecules on different particles that are in close spatial proximity to be considered adjacent and allow for interparticle charge transport. Like in our prior study, a stack of 100 particles and 1% molecular coverage of electrocatalysts are used, but unique to the work herein is that some geometries have more particle overlap and therefore fewer possible molecular positions per particle. This means that in a stack of 100 particles a different number of total molecular positions exists in comparison to the discrete particle structure, which was also used in our prior study. To enable comparable results among geometries, a fixed *percentage* of the total number of dye molecules is simulated to undergo a photoexcitation event, rather than a fixed *number* of dye molecules per stack like in our prior study.

While our prior study focused on simulating different conditions for a simple particle arrangement consisting of an array of isolated spherical semiconductor particle supports, it was limited in its applicability to actual mesoporous thin films because oxidized/reduced molecular charges were physically isolated to a single particle. This meant that oxidized/reduced molecular charges on one particle could only interact with electrocatalysts on that same particle, overall resulting in more restrictive percolation zones than present in actual mesoporous thin films. Performing Monte Carlo simulations where electron-transfer events between particles are allowed to occur is not a new concept[8,26−37] but the detailed functionality and inclusion of discrete dyes and electrocatalysts are unique to our model, therefore enabling a better understanding of design rules for these functional constructs.

Modifications to the Modeling Framework from Our Prior Study. Our model herein assumes that each electrocatalyst requires two oxidized/reduced molecular charges to generate a completely

https://dx.doi.org/10.1021/acsaem.0c00336
ACS Appl. Energy Mater. 2020, 3, 4699−4707

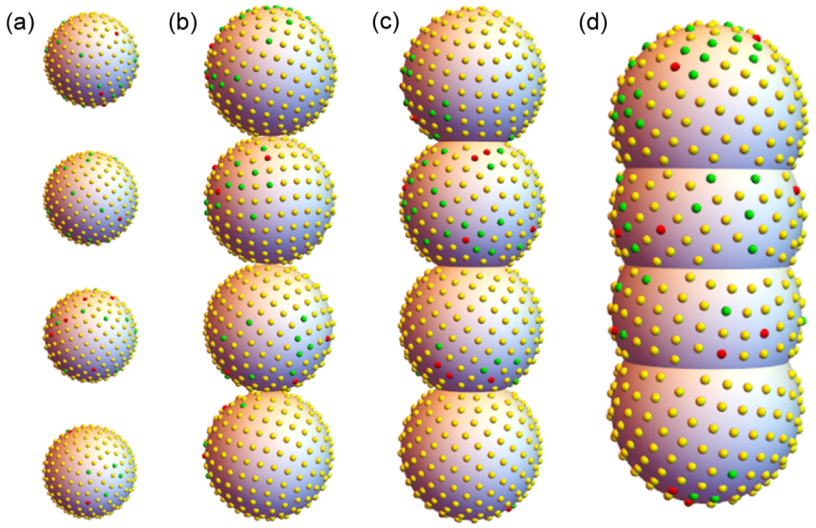

Figure 2. Particle representations of the main three-dimensional structures used in the models: (a) discrete, (b) touching, (c) necked, and (d) rod. Also shown are examples of distributions of ground-state dyes (yellow hemispheres), electrocatalysts (red hemispheres), and photo-oxidized/reduced dyes (green hemispheres).

oxidized/reduced state, which is then assumed to immediately turn over electrocatalytically, and the outcomes of the simulations are reported as mean values obtained from 25 simulations per parameter set. A conclusion from our prior study was that, in the case of simulations that used pulsed-light excitation, the ratio of the following two experimentally relevant time constants (τ_{ratio}) was the independent variable in determining the yield for electrocatalyst turnover and not either one of the time constants alone: time constant for recombination events between charges in the semiconductor and oxidized/reduced surface-anchored molecules (τ_{recomb}) and time constant for self-exchange electron-transfer hopping events between adjacent dyes (τ_{hop}). Therefore, the simulations performed herein used a one-dimensional array of values for τ_{hop} each paired with only one of two different values for τ_{recomb} in order to calculate $\tau_{ratio} = \tau_{recomb}/\tau_{hop}$. This resulted in a parameter space that consisted of 25 distinct time-constant ratios spanning 8 orders of magnitude, 7 of which were formed in duplicate by using each recombination time constant, as shown in Table 1. This parameter space contrasts that used in our prior study where the array of independent variables as τ_{hop} and τ_{recomb} formed a large two-dimensional matrix, consisting of 196 combinations with 42 distinct time-constant ratios spanning ~9 orders of magnitude. While this enabled us to display a detailed three-dimensional sheet plot of the simulation results, it ultimately spanned a similar parameter space of simulated time-constant ratios, which in our previous study was determined to be the more accurate independent variable. The parameter space used herein shortens computation time by simulating fewer combinations with minimal redundancy while also simulating a similar range of time-constant ratios. Some redundancy in the time-constant ratio was intentionally implemented as a test of our previous assumption that the time-constant ratio was the most appropriate independent variable. This redundancy results in two values for the mean turnover yield for several time-constant ratios and clearly illustrates in the figures that the time-constant ratio is the most appropriate independent variable.

Table 1. Modeled Values for τ_{hop} and the Resulting τ_{ratio} Values, Which Equal τ_{recomb}/τ_{hop}

τ_{hop}	τ_{ratio} (using $\tau_{recomb} = 1 \times 10^3$)	τ_{ratio} (using $\tau_{recomb} = 1 \times 10^6$)
1×10^5	1×10^{-2}	1×10^1
5×10^4	2×10^{-2}	2×10^1
2×10^4	5×10^{-2}	5×10^1
1×10^4	1×10^{-1}	1×10^2
5×10^3	2×10^{-1}	2×10^2
2×10^3	5×10^{-1}	5×10^2
1×10^3	1×10^0	1×10^3
5×10^2	2×10^0	2×10^3
2×10^2	5×10^0	5×10^3
1×10^2	1×10^1	1×10^4
5×10^1	2×10^1	2×10^4
2×10^1	5×10^1	5×10^4
1×10^1	1×10^2	1×10^5
5×10^0	2×10^2	2×10^5
2×10^0	5×10^2	5×10^5
1×10^0	1×10^3	1×10^6

Another important difference herein in comparison to our prior study is the process by which molecular sites are assigned. Instead of using Mathematica's built-in tessellation function to create a fixed geometric pattern of positions, a method based on Fibonacci spirals was used to evenly distribute points over the surface of a sphere.[17] The benefits of using Fibonacci spirals are twofold. The greater benefit is that the Fibonacci spiral method allows for any number of points, while the tessellation method always resulted in the same pattern but could accommodate only a few very specific numbers of points. This means that by using Fibonacci spirals, identically sized particles can contain many different point densities or many differently sized particles can contain the same point density. The other benefit of implementing Fibonacci spirals to determine positions on each spherical particle is that molecular positions on each particle are not all relatively the same, which was not the case for the tessellation method. Irrespective, in both cases all positions on each particle are rotated azimuthally and longitudinally based on the center of the particle to create a random relative orientation of molecular positions among particles.

The model utilized herein also includes other differences in comparison to our previous model: (1) Vertical position of the *dye molecule* from the perspective of Figure 2 is used to determine the probability of excitation when the Beer–Lambert law generation profile is operative, instead of the vertical position of the *particle* to which the dye is anchored to like in our prior study; this was a necessary change to accommodate nonlinear particle geometries introduced in this study, yet the Beer–Lambert law generation profile was not used for any simulation results reported herein. (2) Each molecule is considered adjacent to all molecules within a fixed distance from its center, which results in a variable number of adjacent molecular positions, instead of fixing the number of adjacent molecular positions to 5 or 6 like in our prior study; for example,

https://dx.doi.org/10.1021/acsaem.0c00336
ACS Appl. Energy Mater. 2020, 3, 4699–4707

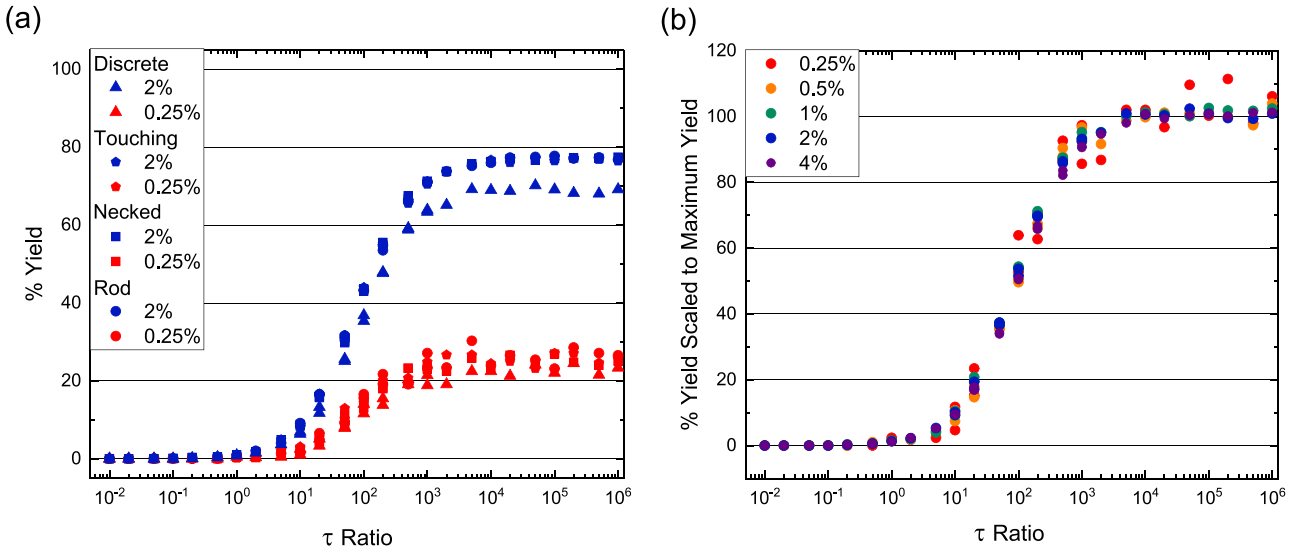

Figure 3. (a) Yield for electrocatalyst turnover as a function of time-constant ratio for each of the four structures depicted in Figure 2 and after the indicated pulsed-laser fluence, represented as the percentage of dyes initially photoexcited. (b) Yield for electrocatalyst turnover normalized to the statistically limiting turnover yield (Figure S2b) as a function of time-constant ratio for the discrete structure and after the indicated pulsed-laser fluence.

this means that molecules located near necking regions at the interface of two particles potentially have more adjacent molecular positions than molecules located far from necking regions, which results in between 6 to 8 adjacent molecular positions depending on the local geometry. (3) Percolation zones are identified for each molecular position because, for many structures, particles are in physical contact and therefore adjacent molecules may be located on other particles, instead of assuming that electron transfer can only occur to any molecules on a single particle like in our prior study; a percolation zone consists of molecular positions that are accessible for oxidation/reduction from a given oxidized/reduced molecule, and for more complex three-dimensional structures many percolation zones do not contain all molecular positions on a particle but often contain molecular positions on several adjacent particles. (4) Photoexcitations that occur in percolation zones that contain zero electrocatalysts or photoexcitations that occur in too few of a number to result in electrocatalyst turnover in a percolation zone are identified at the beginning of the simulation, and the simulation is terminated once only oxidized/reduced molecular charges from these photoexcitations remain, instead of removing these photoexcitations from the outset like in our prior study; these oxidized/reduced molecules must remain present during the simulation because even if an oxidized/reduced molecule in a percolation zone cannot possibly result in electrocatalyst turnover, the molecule and its matched charge in the semiconducting support affect recombination on the entire particle, and another percolation zone may exist on the particle that contains oxidized/reduced molecules that are able to drive electrocatalyst turnover.

Modifications to the Modeling Framework for Simulations of Two-Dimensional Structures. Simulations were also performed using two-dimensional planar structures, where several significant modifications were made to the above protocols. One change is that geometric considerations such as photon polarization and the Beer–Lambert law generation profile are no longer considered with the planar surfaces because they are two-dimensional. Another change is that periodic boundary conditions are used with the planar surfaces such that self-exchange electron-transfer events can occur from one side of a planar surface to another, meaning that opposite edges (right and left, top and bottom) are considered adjacent. The final major change is that electron density is distributed homogeneously across the planar surfaces. This is included to realistically account for the second-order recombination behavior based on the concentration of charges; however, simply treating the surface as one large particle results in an extremely large recombination rate. This is because the planar surface is akin to a single particle, yet the hexagonal grid has 25 088 molecular positions (as a 224 row × 112 column grid) and the square grid has 24 964 molecular positions (as a 158 × 158 grid), each to mimic the 25 000 molecular positions in the discrete particle structure where there are only 250 molecular positions per particle. To correct for this physically unrealistic rapid rate of recombination, the electron density for the planar surfaces is determined by dividing the concentration of charges by the number of rows on the surface.

RESULTS AND DISCUSSION

The primary focus of our work was to compare across several support geometries the turnover yield of electrocatalysts that require two redox events for turnover as a function of the ratio of two experimentally relevant time constants ($\tau_{ratio} = \tau_{recomb}/\tau_{hop}$). These experimentally relevant time constants are for the processes of recombination between charges in the semiconductor support and oxidized/reduced molecules anchored to the surface of the support geometry (τ_{recomb}) and self-exchange electron transfer between adjacent dye molecules anchored to the surface of the support geometry (τ_{hop}). In our prior study,[25] we determined that this time-constant ratio was the independent variable that dictated the turnover yield based on simulations using an analogous modeling framework to that used herein. We chose to simulate that electrocatalysts only require two charges for turnover because that condition is most relevant to dye-sensitized solar cells that utilize the iodide/triiodide redox mediator; however, it is equally as relevant to other photoelectrochemical constructs that, for example, drive the two-electron-transfer hydrogen-evolution reaction or the two-electron-transfer chlorine evolution reaction, among others.

Effect of Pulsed-Laser Fluence. The yield for electrocatalyst turnover was first analyzed for all four structures shown in Figure 2 as a function of time-constant ratio, with results shown in Figure 3a after high pulsed-laser fluence (blue) and low pulsed-laser fluence (red), and with additional intermediate fluence conditions shown in Figure S1. These data indicate that larger pulsed-laser fluence results in larger electrocatalytic turnover yield independent of the structure.

https://dx.doi.org/10.1021/acsaem.0c00336
ACS Appl. Energy Mater. 2020, 3, 4699–4707

A larger turnover yield at higher fluence is a consequence of the statistics of randomly assigning photogenerated oxidized/reduced molecular charges to electrocatalysts. When the data are normalized for this effect (Figures 3b and S2), there are no significant differences in turnover yield as a function of time-constant ratio across several pulsed-laser fluences. The data in Figure 3 also show that the limiting turnover yield occurs for a time-constant ratio between 10^3 and 10^4 for all simulated pulsed-laser fluences, suggesting that mesoporous photoelectrochemical constructs containing surface-confined light-absorbing and electrocatalytic units should aim to have time constants that result in these ratios. Notably, only under the high-fluence condition is there a significant difference in limiting turnover yield based on scaffold structure (Figure 3a), with a significantly smaller predicted limiting turnover yield for the discrete particle structure than the touching, necked, and rod structures, which are all same within the error of the simulations. A smaller limiting turnover yield for the discrete particle structure is observed because it is possible to photoexcite dyes on particles that do not contain electrocatalysts, meaning that those photoexcitations cannot contribute to electrocatalyst turnover. On all other structures there are surface-confined electron transport pathways that connect every molecule to every other molecule, meaning that even for photoexcitations that occur several particles away from an electrocatalyst, in the limit of large time-constant ratio, the electrocatalyst will be oxidized/reduced. To confirm that in the limit of large time-constant ratio electron-transfer events occur between adjacent particles, the average number of distinct particles visited by each photogenerated charge was calculated as a function of time-constant ratio for each of the four structures (Figure S3). In addition, the turnover yield does not seem to depend on the connectedness of a structure in terms of necking and percolation pathways. For example, the touching structure has very few interparticle percolation pathways, yet within the error of the simulations, its yield for electrocatalyst turnover is the same as the rod structure where many percolation pathways exist.

Effect of Photon Polarization. One measurement that yields vastly different results among the structures shown in Figure 2 is the calculated time-dependent spectroscopic anisotropy. If the incident pulsed-laser light is simulated to be linearly polarized, dye molecules whose transition dipole moment is collinear with the electric field vector of the incident light are more likely to absorb a photon. This effect was included in the model via a weighting factor that determined the probability for photoexcitation of dye molecules based on their orientation relative to a chosen vector that represented the direction of electric field polarization of the photon as follows:

$$W = \cos^2 \theta \tag{1}$$

where W is the relative weight for the probability of excitation for a given dye molecule, and θ is the angle between the electric field polarization vector of the photon and the transition dipole moment of each dye. Dye molecules were assumed to have transition dipole moments oriented radially from the center of the particle to which they were anchored. This weighting factor creates an anisotropic distribution of photoexcitation events with an anisotropy that changes over time as oxidized/reduced molecular charges transfer along the surface of the structure through self-exchange electron-transfer events. The spectroscopically observable anisotropy is calculated as the average of the anisotropy contribution of each oxidized/reduced molecular charge as follows

$$r = \frac{3\cos^2 \theta - 1}{2} \tag{2}$$

where r is the contribution to the anisotropy. θ could be defined differently in the case that the anisotropy relative to another vector was of interest or that the transition dipole moment vector of the dye changed after absorbing a photon or becoming oxidized/reduced. For simplicity, the same θ value is used to calculate the probability of photoexcitation and the anisotropy. Figure 4 shows how the anisotropy transients

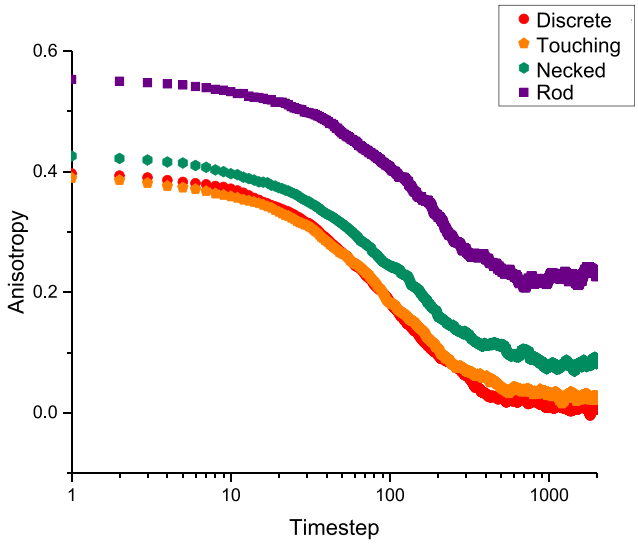

Figure 4. Calculated spectroscopic anisotropy over time for each of the four structures depicted in Figure 2. In all cases, the coverage of electrocatalysts and percentage of photoexcitations were each assumed to be 1% of the molecular surface, the recombination time constant was set equal to 1 ms, and the hopping time constant was set equal to 1 μs, meaning a time-constant ratio of 10^3.

change over time and differ among the structures, where the electric field polarization vector of the photon is horizontal from the perspective of Figure 2. For the discrete particle structure, which consists of isolated spheres, the initial anisotropy value is equal to the theoretical short-term value of 0.4 and approaches zero over time via an exponential decay. However, the connected structures have some amount of particle necking, and therefore some molecular positions are left unoccupied near the poles along the vertical axis from the perspective of Figure 2, resulting in larger initial and long-time anisotropy values, albeit with changes that occur via a time-dependent rate that is independent of the structure within the error of the simulations. This means that to obtain experimental data that are only influenced by reaction kinetics, like electron transfer or energy transfer, one must use polarizers positioned either at the magic angle (54.7°) with respect to the electric field polarization vector of the incident light or at several known angles that are then used to mathematically compute the magic angle kinetics and spectra. Data from our simulations also suggest that anisotropy values can converge to nonzero values at long times, and this behavior may be indicative of a nonspherical structure. Notwithstanding, simulations of turnover yield are not influenced significantly by the use of incident light that is linearly polarized (Figure S4).

https://dx.doi.org/10.1021/acsaem.0c00336
ACS Appl. Energy Mater. 2020, 3, 4699−4707

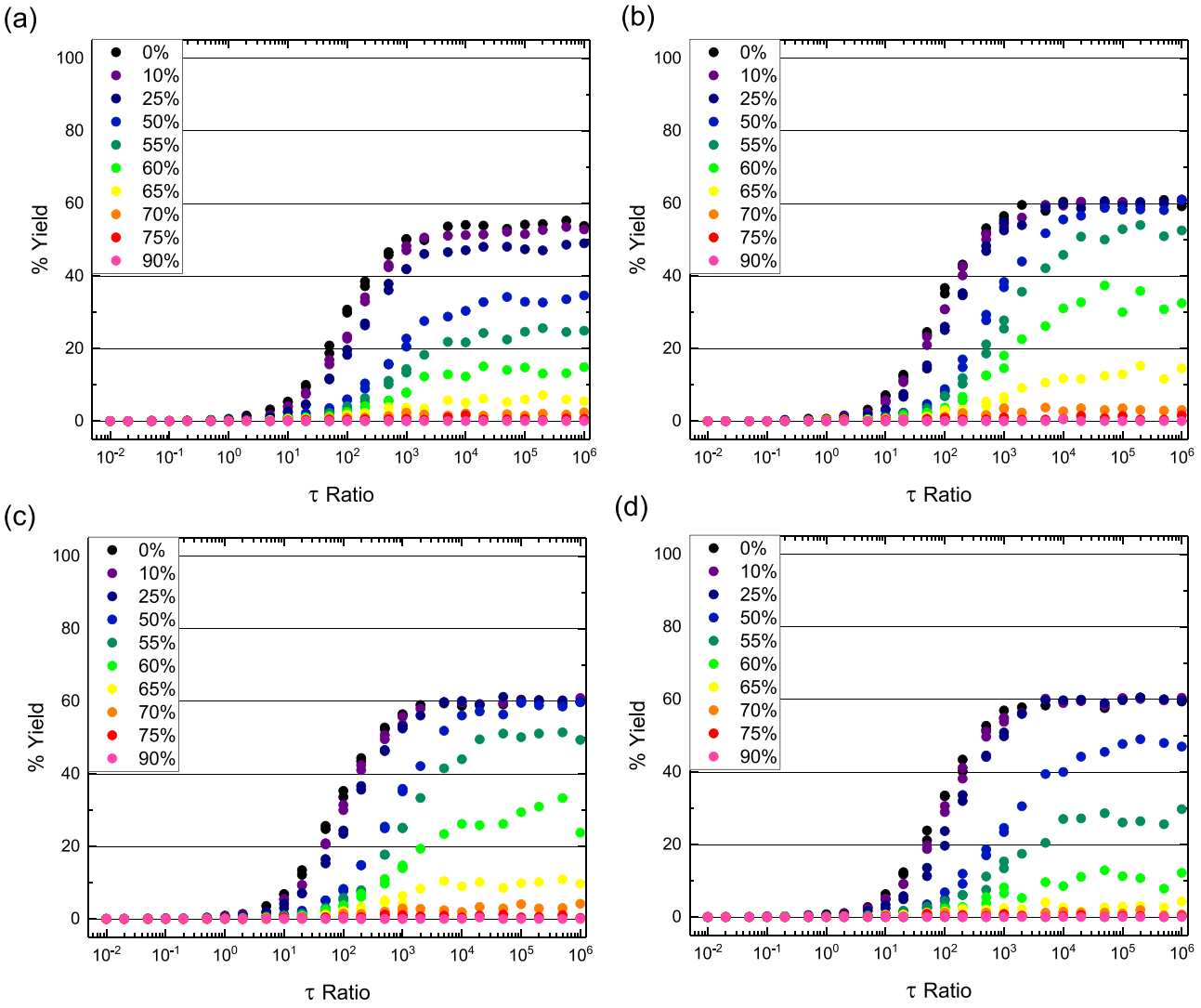

Figure 5. Yield for electrocatalyst turnover as a function of time-constant ratio after 1% of the dyes are initially photoexcited and with the indicated percentage of vacant molecular positions for each of the four structures depicted in Figure 2: (a) discrete, (b) touching, (c) necked, and (d) rod.

Effect of Vacant Molecular Positions. Experimentally, binding molecular dyes to a mesoporous thin film of nanocrystallites is an imperfect process that results in variability in local surface coverages. Therefore, we also investigated the effect that total molecular coverage, and thus percolation, has on turnover yield (Figure 5). A percolation network is important so that oxidized/reduced molecular charges resulting from photoexcitation are able to transport to electrocatalysts. Therefore, a certain percentage of potential molecular positions was chosen to be vacant before molecular positions for electrocatalysts were selected. For example, in a discrete particle structure with 250 molecular positions over 100 discrete particles that contain 50% vacant molecular positions, 1% electrocatalyst coverage, and 1% dye photoexcitation, there are 12 500 sites that are randomly selected to be vacant, 125 of the remaining sites are chosen to be catalyst sites, and 124 of the remaining sites (rounded from 123.75) are chosen to be initially photoexcited dyes. One observation from the results of these simulations is that breakdown of the percolation network does not begin to result in a significant decrease in the turnover yield until nearly 50% of the molecular positions are vacant and that even at that coverage, oxidized/reduced molecular charges are still able to transport to electrocatalysts for the touching and necked structures, when charge recombination is slow. This indicates that even at 50% molecular vacancies, a percolation network can still exist but that it may not be direct and so a molecular charge may require many more self-exchange electron-transfer events before reaching an electrocatalyst. The results shown in Figure 5 also suggest that the majority of the percolation pathways are removed at between ∼55% and ∼60% molecular vacancies but that the percolation network is not entirely removed even when ∼70% of the molecular positions are vacant.

Another observation is that the discrete particle structure is affected to a greater extent by the presence of a large number of molecular vacancies (Figure 5a). Even at only 10−25% molecular vacancies, the limiting turnover yield decreases noticeably in comparison to when zero molecular vacancies are present. This behavior is observed because the discrete particle structure is already made up of a number of smaller percolation zones, i.e., each particle, and so the structure is more susceptible to the breakdown of percolation networks. This is in opposition to the connected structures where an oxidized/reduced molecule that has zero electrocatalysts on the same particle may still be able to oxidize/reduce an electrocatalyst if it can transport by self-exchange electron-transfer events to

https://dx.doi.org/10.1021/acsaem.0c00336
ACS Appl. Energy Mater. 2020, 3, 4699−4707

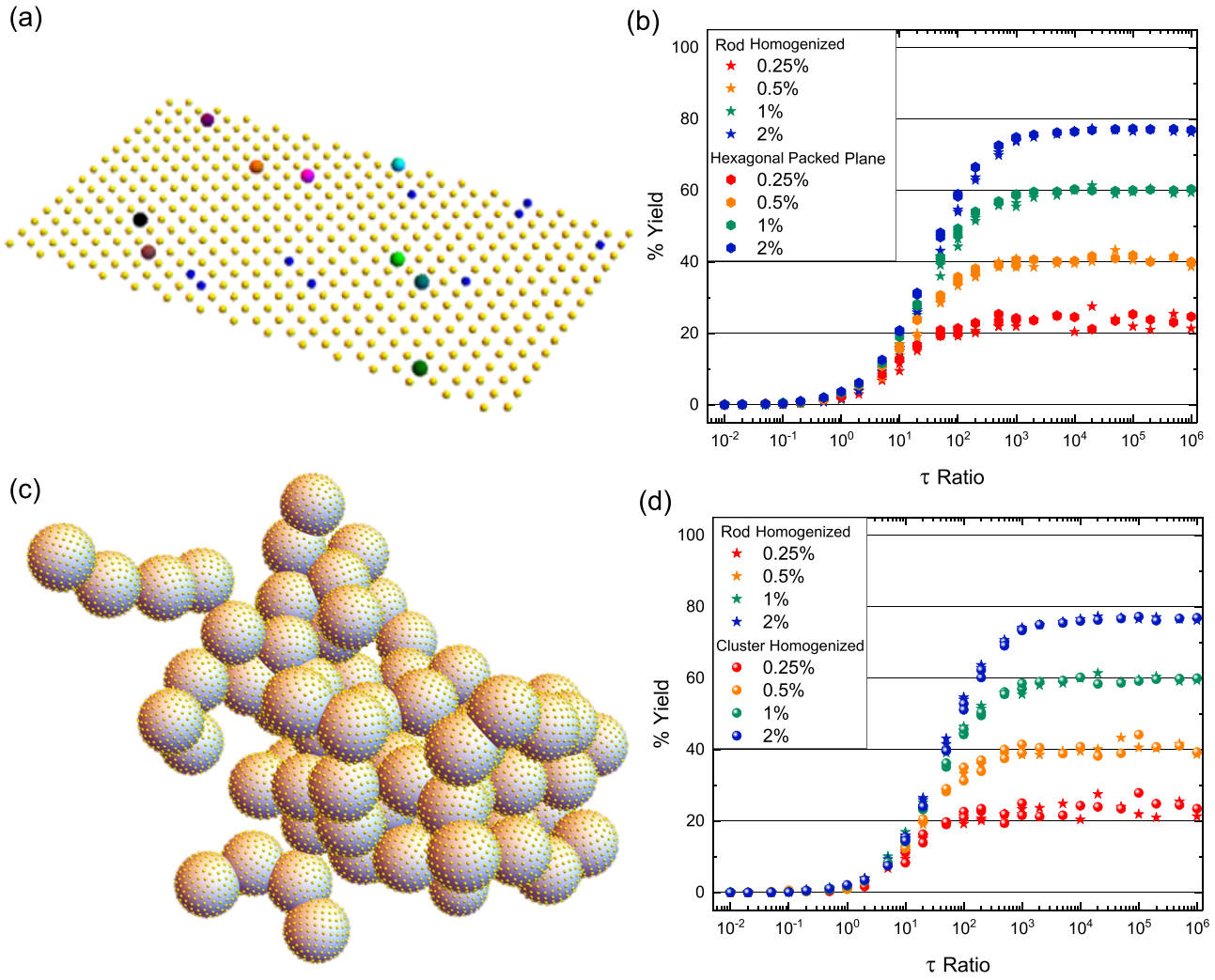

Figure 6. (a) Portion of the planar surface structure consisting of a hexagonal grid of molecular positions that each have six adjacent molecular positions and with a random distribution of ground-state dyes (yellow spheres), electrocatalysts (blue spheres), and photo-oxidized/reduced dyes (larger colored spheres). (b) Yield for electrocatalyst turnover as a function of time-constant ratio for the three-dimensional rod structure and the two-dimensional planar surface shown in panel a, each with homogenized electron density and after the indicated pulsed-laser fluence, represented as the percentage of dyes initially photoexcited. (c) Clustered structure consisting of 100 particles that overlap each other by distances equal to 0–50% of their radii, resulting in 19 095 molecular positions (yellow hemispheres). (d) Yield for electrocatalyst turnover as a function of time-constant ratio for the rod structure and the clustered structure shown in panel c, each with homogenized electron density and after the indicated pulsed-laser fluence.

another particle. Interestingly, of the connected structures, the rod structure has a significantly smaller turnover yield at a moderate coverage of molecular vacancies (50–65%) than the other connected structures, an observation that is analyzed in greater detail in the text associated with Figure S5.

Effect of Simplifying versus Complicating the Surface Geometry. The major conclusion from the results thus far is that the majority of variables do not significantly impact the yield for electrocatalyst turnover as a function of time-constant ratio. This led us to question whether the added complexity in our model actually results in the observation of more significant outcomes or whether a simpler geometry would be equivalent. To this end, two-dimensional planar structures were modeled and simulated using a protocol that was nearly the same as that used for the three-dimensional structures, but with several significant modifications that included not including effects due to photon polarization, including periodic boundary conditions, and homogenizing electron density over the entire surface and scaling the number of charges by the number of rows in the surface grid. To make comparisons between results obtained from simulations of the two-dimensional planar surfaces and the three-dimensional structures shown in Figure 2, simulations were performed using homogenized electron density for the three-dimensional structures and results are shown in Figure S6, where comparisons made to the analogous results obtained using nonhomogenized electron density (Figure S1) indicate very minor changes in turnover yield as a function of time-constant ratio.

In addition to the planar surface shown in Figure 6a, where molecular positions were aligned along a hexagonal grid, another planar surface was simulated where molecular positions were aligned along a square grid (Figure S7). Comparison of the results using homogenized electron density for the three-dimensional discrete particle structure, the three-dimensional rod structure, and all two-dimensional planar

https://dx.doi.org/10.1021/acsaem.0c00336
ACS Appl. Energy Mater. 2020, 3, 4699–4707

surfaces (Figures 6b and S9) suggests that the number of adjacent molecular positions is an important parameter in predicting the yield for electrocatalyst turnover and that the overall behavior in turnover yield as a function of time-constant ratio and the value of the limiting turnover yield at large values of the time-constant ratio are in general independent of the dimension of the structure used to perform the simulation.

In contrast to the simplified two-dimensional planar surfaces, a three-dimensional clustered structure was created that simulates a more realistic and complex mesoporous thin film (Figure 6c). The goal of using the clustered structure was to determine whether any additional behavior could be observed or information could be obtained by complicating the structure in a more realistic manner than the three-dimensional structures shown in Figure 2. Comparison of the results using homogenized electron density for the two-dimensional planar surface with a hexagonal grid, the three-dimensional rod structure, and the three-dimensional clustered structure (Figure 6b,d) indicates that all three very different geometries produce nearly the same yields for electrocatalyst turnover as a function of time-constant ratio. This suggests that the complexity of the three-dimensional structures shown in Figure 2 and the clustered structure shown in Figure 6c, versus the two-dimensional planar structures, is likely not necessary to accurately predict turnover yields as a function of time-constant ratio. Overall, results from these simulations indicate that as long as distributions of molecules can be arranged on a surface where the number of adjacent molecular positions is consistent with experimental arrangements, the expected empirical turnover yield as a function of the empirical values that make up the time-constant ratio, i.e., τ_{hop} and τ_{recomb}, can be reasonably approximated using our numerical models and simulations.

CONCLUSIONS

This work continued the development of an advanced model for charge transport across the surface of dye and cocatalyst-modified mesoporous materials. When charge recombination between the semiconducting mesoporous thin film and an oxidized/reduced dye or electrocatalyst was modeled to be slow, results from simulations indicate that electrocatalytic turnover yield was larger for structures containing particles that were in physical contact due to interparticle self-exchange electron transfer. However, changing the degree to which particle surfaces overlapped did not have a significant effect on turnover yield. Results from simulations also indicate that the use of linearly polarized light to photoexcite dye molecules has little effect on turnover yield but that the initial magnitude of the simulated spectroscopic anisotropy signal is drastically different when simulations are performed using spherical structures versus rodlike structures. Moreover, when 50−65% of possible molecular positions are vacant, percolation networks are more effective at transporting molecular charges and resulting in electrocatalytic turnover for structures consisting of nanoparticles that barely touch or are partially necked in comparison to rodlike structures. Simulations also suggest that use of models consisting of complex geometries that more closely resemble mesoporous materials used in experiments, versus a simple two-dimensional planar grid, provides minimal additional information or benefit regarding the yield for electrocatalyst turnover as a function of the ratio of the electron-transfer time constant for self-exchange reactions and charge recombination time constant between the semiconducting mesoporous thin film and an oxidized/reduced surface-confined dye or electrocatalyst.

ASSOCIATED CONTENT

Supporting Information

The Supporting Information is available free of charge at https://pubs.acs.org/doi/10.1021/acsaem.0c00336.

Additional simulation results showing yield for electrocatalyst turnover as a function of time-constant ratio, three-dimensional or two-dimensional structure type, and pulsed-laser fluence for (i) linearly polarized light versus unpolarized light, (ii) 0% and 50% molecular vacancies, (iii) electron density homogenized across all positions versus electron density fixed to particles that have an oxidized/reduced molecular charge on them, (iv) average number of unique particles visited by an individual oxidized/reduced molecular charge during its lifetime as a function of time-constant ratio and structure type, (v) number of excitations per percolation zone as a function of the percentage of vacant molecular positions, and (vi) portion of the planar surface structure consisting of a square grid of molecular positions (PDF)

AUTHOR INFORMATION

Corresponding Author

Shane Ardo − *Department of Chemistry, Department of Materials Science & Engineering, and Department of Chemical & Biomolecular Engineering, University of California Irvine, Irvine, California 92697-2025, United States;* orcid.org/0000-0001-7162-6826; Email: ardo@uci.edu

Author

Kevin Tkaczibson − *Department of Materials Science & Engineering, University of California Irvine, Irvine, California 92697-2025, United States*

Complete contact information is available at: https://pubs.acs.org/10.1021/acsaem.0c00336

Notes

The authors declare no competing financial interest.

ACKNOWLEDGMENTS

This work was supported by the National Science Foundation under CHE—1566160 and the School of Physical Sciences at the University of California Irvine.

REFERENCES

(1) Swierk, J. R.; Mallouk, T. E. Design and Development of Photoanodes for Water-Splitting Dye-Sensitized Photoelectrochemical Cells. *Chem. Soc. Rev.* **2013**, *42*, 2357−2387.

(2) Ashford, D. L.; Gish, M. K.; Vannucci, A. K.; Brennaman, M. K.; Templeton, J. L.; Papanikolas, J. M.; Meyer, T. J. Molecular Chromophore−Catalyst Assemblies for Solar Fuel Applications. *Chem. Rev.* **2015**, *115*, 13006−13049.

(3) Ardo, S.; Meyer, G. J. Photodriven Heterogeneous Charge Transfer with Transition-Metal Compounds Anchored to TiO_2 Semiconductor Surfaces. *Chem. Soc. Rev.* **2009**, *38*, 115−164.

(4) Hu, K.; Meyer, G. J. Lateral Intermolecular Self-Exchange Reactions for Hole and Energy Transport on Mesoporous Metal Oxide Thin Films. *Langmuir* **2015**, *31*, 11164−11178.

(5) Barzykin, A. V.; Tachiya, M. Mechanism of Molecular Control of Recombination Dynamics in Dye-Sensitized Nanocrystalline Semiconductor Films. *J. Phys. Chem. B* **2004**, *108*, 8385−8389.
(6) Bisquert, J. Hopping Transport of Electrons in Dye-Sensitized Solar Cells. *J. Phys. Chem. C* **2007**, *111*, 17163−17168.
(7) Higgins, G. T.; Bergeron, B. V.; Hasselmann, G. M.; Farzad, F.; Meyer, G. J. Intermolecular Energy Transfer across Nanocrystalline Semiconductor Surfaces. *J. Phys. Chem. B* **2006**, *110*, 2598−2605.
(8) Hu, K.; Robson, K. C. D.; Beauvilliers, E. E.; Schott, E.; Zarate, X.; Arratia-Perez, R.; Berlinguette, C. P.; Meyer, G. J. Intramolecular and Lateral Intermolecular Hole Transfer at the Sensitized TiO_2 Interface. *J. Am. Chem. Soc.* **2014**, *136*, 1034−1046.
(9) Ardo, S.; Meyer, G. J. Direct Observation of Photodriven Intermolecular Hole Transfer across TiO_2 Nanocrystallites: Lateral Self-Exchange Reactions and Catalyst Oxidation. *J. Am. Chem. Soc.* **2010**, *132*, 9283−9285.
(10) Ardo, S.; Meyer, G. J. Characterization of Photoinduced Self-Exchange Reactions at Molecule−Semiconductor Interfaces by Transient Polarization Spectroscopy: Lateral Intermolecular Energy and Hole Transfer across Sensitized TiO_2 Thin Films. *J. Am. Chem. Soc.* **2011**, *133*, 15384−15396.
(11) Anta, J. A.; Mora-Seró, I.; Dittrich, T.; Bisquert, J. Interpretation of Diffusion Coefficients in Nanostructured Materials from Random Walk Numerical Simulation. *Phys. Chem. Chem. Phys.* **2008**, *10*, 4478−4485.
(12) Anta, J. A. Random Walk Numerical Simulation for Solar Cell Applications. *Energy Environ. Sci.* **2009**, *2*, 387−392.
(13) Moia, D.; Szumska, A.; Vaissier, V.; Planells, M.; Robertson, N.; O'Regan, B. C.; Nelson, J.; Barnes, P. R. F. Interdye Hole Transport Accelerates Recombination in Dye Sensitized Mesoporous Films. *J. Am. Chem. Soc.* **2016**, *138*, 13197−13206.
(14) Chen, H. Y.; Ardo, S. Direct Observation of Sequential Oxidations of a Titania-Bound Molecular Proxy Catalyst Generated through Illumination of Molecular Sensitizers. *Nat. Chem.* **2018**, *10*, 17−23.
(15) Trammell, S. A.; Yang, J.; Sykora, M.; Fleming, C. N.; Odobel, F.; Meyer, T. J. Molecular Energy Transfer across Oxide Surfaces. *J. Phys. Chem. B* **2001**, *105*, 8895−8904.
(16) Anta, J. A.; Morales-Flórez, V. Combined Effect of Energetic and Spatial Disorder on the Trap-Limited Electron Diffusion Coefficient of Metal-Oxide Nanostructures. *J. Phys. Chem. C* **2008**, *112*, 10287−10293.
(17) Ansari-Rad, M. Dye Regeneration Kinetics in Dye-Sensitized Solar Cell: Long-Range Charge-Transfer Effects. *J. Phys. Chem. C* **2016**, *120*, 9000−9006.
(18) Nelson, J. Continuous-Time Random-Walk Model of Electron Transport in Nanocrystalline TiO_2 Electrodes. *Phys. Rev. B* **1999**, *59*, 15374−15380.
(19) Nelson, J.; Haque, S.; Klug, D.; Durrant, J. Trap-Limited Recombination in Dye-Sensitized Nanocrystalline Metal Oxide Electrodes. *Phys. Rev. B* **2001**, *63*, No. 205321.
(20) Nelson, J.; Chandler, R. E. Random Walk Models of Charge Transfer and Transport in Dye Sensitized Systems. *Coord. Chem. Rev.* **2004**, *248*, 1181−1194.
(21) Vaissier, V.; Mosconi, E.; Moia, D.; Pastore, M.; Frost, J. M.; De Angelis, F.; Barnes, P. R. F.; Nelson, J. Effect of Molecular Fluctuations on Hole Diffusion within Dye Monolayers. *Chem. Mater.* **2014**, *26*, 4731−4740.
(22) Ansari-Rad, M.; Anta, J. A.; Bisquert, J. Interpretation of Diffusion and Recombination in Nanostructured and Energy-Disordered Materials by Stochastic Quasiequilibrium Simulation. *J. Phys. Chem. C* **2013**, *117*, 16275−16289.
(23) Barzykin, A. V.; Tachiya, M. Mechanism of Charge Recombination in Dye-Sensitized Nanocrystalline Semiconductors: Random Flight Model. *J. Phys. Chem. B* **2002**, *106*, 4356−4363.
(24) Katoh, R.; Furube, A.; Barzykin, A. V.; Arakawa, H.; Tachiya, M. Kinetics and Mechanism of Electron Injection and Charge Recombination in Dye-Sensitized Nanocrystalline Semiconductors. *Coord. Chem. Rev.* **2004**, *248*, 1195−1213.
(25) Tkaczibson, K.; Ardo, S. Numerical Monte Carlo Simulations of Charge Transport across the Surface of Dye and Cocatalyst Modified Spherical Nanoparticles under Conditions of Pulsed or Continuous Illumination. *Sustainable Energy Fuels* **2019**, *3*, 1573−1587.
(26) Benkstein, K. D.; Kopidakis, N.; van de Lagemaat, J.; Frank, A. J. Influence of the Percolation Network Geometry on Electron Transport in Dye-Sensitized Titanium Dioxide Solar Cells. *J. Phys. Chem. B* **2003**, *107*, 7759−7767.
(27) Gonzalez-Vazquez, J. P.; Bigeriego, G.; Anta, J. A. Influence of the Charge Generation Profile on the Collection Efficiency of Nanostructured Solar Cells: A Random Walk Numerical Simulation Study. *Mol. Simul.* **2012**, *38*, 1242−1250.
(28) Liu, B.; Li, Z.; Zhao, X. Correlation of Electron Transport and Photocatalysis of Nanocrystalline Clusters Studied by Monte-Carlo Continuity Random Walking. *Phys. Chem. Chem. Phys.* **2015**, *17*, 5265−5273.
(29) Gonzalez-Vazquez, J. P.; Anta, J. A.; Bisquert, J. Determination of the Electron Diffusion Length in Dye-Sensitized Solar Cells by Random Walk Simulation: Compensation Effects and Voltage Dependence. *J. Phys. Chem. C* **2010**, *114*, 8552−8558.
(30) Gonzalez-Vazquez, J. P.; Morales-Flórez, V.; Anta, J. A. How Important Is Working with an Ordered Electrode to Improve the Charge Collection Efficiency in Nanostructured Solar Cells? *J. Phys. Chem. Lett.* **2012**, *3*, 386−393.
(31) Ansari-Rad, M.; Abdi, Y.; Arzi, E. Monte Carlo Random Walk Simulation of Electron Transport in Dye-Sensitized Nanocrystalline Solar Cells: Influence of Morphology and Trap Distribution. *J. Phys. Chem. C* **2012**, *116*, 3212−3218.
(32) Abdi, N.; Abdi, Y.; Nedaaee Oskoee, E.; Sajedi, M. Electron Diffusion in Trap-Contained 3D Porous Nanostructure: Simulation and Experimental Investigation. *J. Nanopart. Res.* **2014**, *16*, No. 2308.
(33) Abdi, N.; Abdi, Y.; Alemipour, Z.; NedaaeeOskoee, E. Chemical Diffusion Coefficient in Dye Sensitized Solar Cells as a Function of Porosity and Surface Roughness. *Sol. Energy* **2016**, *135*, 506−511.
(34) Koochi, H.; Ebrahimi, F. Geometrical Effects on the Electron Residence Time in Semiconductor Nano-Particles. *J. Chem. Phys.* **2014**, *141*, No. 094702.
(35) Ansari-Rad, M.; Anta, J. A.; Arzi, E. Conditions for Diffusion-Limited and Reaction-Limited Recombination in Nanostructured Solar Cells. *J. Chem. Phys.* **2014**, *140*, No. 134702.
(36) Ansari-Rad, M.; Abdi, Y.; Arzi, E. Simulation of Non-Linear Recombination of Charge Carriers in Sensitized Nanocrystalline Solar Cells. *J. Appl. Phys.* **2012**, *112*, No. 074319.
(37) Cass, M. J.; Walker, A. B.; Martinez, D.; Peter, L. M. Grain Morphology and Trapping Effects on Electron Transport in Dye-Sensitized Nanocrystalline Solar Cells. *J. Phys. Chem. B* **2005**, *109*, 5100−5107.
(38) Tkaczibson, K. Stochastic Models of Photoexcitation & Charge Accumulation for Solar Energy Conversion. Ph.D. Dissertation, University of California Irvine: Irvine, CA, 2019.

https://dx.doi.org/10.1021/acsaem.0c00336
ACS Appl. Energy Mater. 2020, 3, 4699−4707